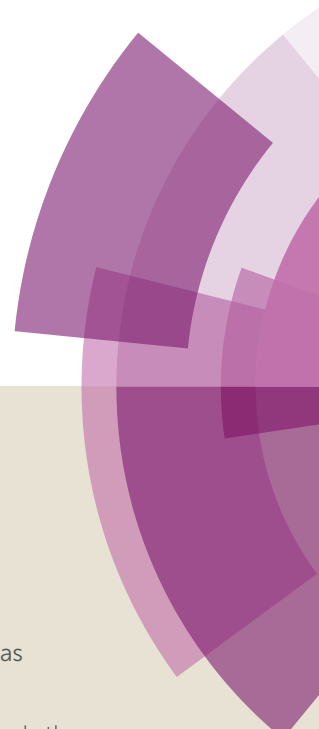
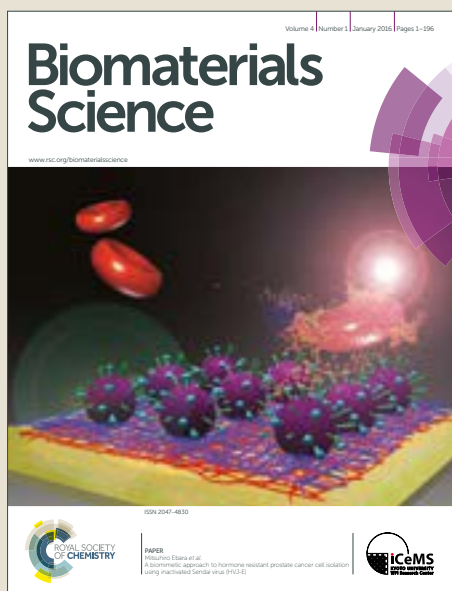


Biomaterials Science

Accepted Manuscript



This article can be cited before page numbers have been issued, to do this please use: C. Simitzi, P. K. Harimech, S. Spanou, C. Lanara, A. Heuer-Jungemann, A. Manousaki, C. Fotakis, A. Ranella, A. G. Kanaras and E. Stratakis, *Biomater. Sci.*, 2018, DOI: 10.1039/C7BM00904F.



This is an Accepted Manuscript, which has been through the Royal Society of Chemistry peer review process and has been accepted for publication.

Accepted Manuscripts are published online shortly after acceptance, before technical editing, formatting and proof reading. Using this free service, authors can make their results available to the community, in citable form, before we publish the edited article. We will replace this Accepted Manuscript with the edited and formatted Advance Article as soon as it is available.

You can find more information about Accepted Manuscripts in the [author guidelines](#).

Please note that technical editing may introduce minor changes to the text and/or graphics, which may alter content. The journal's standard [Terms & Conditions](#) and the ethical guidelines, outlined in our [author and reviewer resource centre](#), still apply. In no event shall the Royal Society of Chemistry be held responsible for any errors or omissions in this Accepted Manuscript or any consequences arising from the use of any information it contains.

Cells on hierarchically-structured platforms hosting functionalized nanoparticles

Chara Simitzi^a, Pascal Harimech^b, Syrago Spanou^{a,c}, Christina Lanara^{a,d}, Amelie Heuer Jungemann^b, Aleka Manousaki^a, Costas Fotakis^{a,c}, Anthi Ranella^a, Antonios G. Kanaras^{b,f}, Emmanuel Stratakis^{a,d}

Affiliations

a Foundation for Research and Technology-Hellas (F.O.R.T.H.), Institute of Electronic Structure and Laser (I.E.S.L.), Heraklion, Greece

b Physics and Astronomy, Faculty of Physical Sciences and Engineering, University of Southampton, UK

c Department of Biology, University of Crete, Heraklion, Greece

d Department of Materials Science and Technology, University of Crete, Heraklion, Greece

e Department of Physics, University of Crete, Heraklion, Greece

f Institute for Life Sciences, University of Southampton, UK

Abstract

In this work, we report on a novel approach to develop hierarchically-structured cell culture platforms incorporating functionalized gold nanoparticles (AuNPs). In particular, the hierarchical substrates comprise primary pseudo-periodic arrays of silicon microcones combined with a secondary nanoscale pattern of homogeneously deposited AuNPs terminated with bio-functional moieties. AuNPs with various functionalities (i.e. oligopeptides, small molecules and oligomers) were successfully attached onto the microstructures. Experiments with PC12 cells on the hierarchical substrates incorporating AuNPs carrying the RGD peptide showed an impressive growth and NGF-induced differentiation of the PC12 cells, compared to that on the NPs-free, bare, micropatterned substrates. The exploitation of the developed methodology for the binding of AuNPs as carriers of specific bio-functional moieties onto micropatterned culture substrates for cell biology studies is envisaged.

1. Introduction

Gold nanoparticles (AuNPs) are employed in various biomedical applications. Their broad use is attributed to their unique properties, which are either directly or indirectly correlated with their size. For example, the optical and thermal properties of gold nanoparticles are exploited in diagnostics, including bioimaging and biosensing (surface-enhanced optical-spectroscopical properties/absorption and scattering) (reviewed in ¹) and in photodynamic therapy (optical heating and photochemical reaction generation) (reviewed in ^{1,2}). Due to their small and tunable size, their ease of functionalization/bioconjugation and their high surface-to-volume ratio, AuNPs are exploited in drug delivery systems ^{1,3-6}, as novel contrast agents ² and as coatings of medical implants ⁷.

There is an immense need to understand the cells/tissues-nanoparticles interactions for each application. The majority of the *in vitro* studies so far include cells grown on petri dishes and incubated with functional nanoparticles. These studies focus on the effect of different nanoparticles parameters (e.g. size, shape,

functionality, concentration, etc.) on cell toxicity, and generally they investigate whether cell functions are somehow altered by the presence of nanoparticles (reviewed in ⁸) ⁹. Such studies provide important information regarding the cell-nanoparticles interactions and the nanoparticle uptake by the cells, which are critical in applications, such as drug delivery systems and intracellular imaging ^{8,10}. However, they cannot provide an insight into the condition where cells are exposed to nanoparticles attached on a functional surface, as in the case of implants or bioanalytical sensors. Thus, new types of culture platforms are developed in order to study the basolateral cells-nanoparticles interactions.

Two dimensional substrates with attached gold and other plasmonic nanoparticles, defined as plasmonic substrates, have been recently introduced (reviewed in ¹¹). Plasmonic platforms are investigated for their potential in label-free sensing of biomolecules and living cells ¹². Plasmonic nanoparticles assembled onto a substrate enable surface plasmon phenomena, which can enhance the Raman signal of cells grown on them measured by surface enhanced raman scattering (SERS) spectroscopy ¹². Furthermore, novel cell culture platforms comprising nanopatterns of gold nanoparticles with immobilized oligopeptides or even whole proteins, such as receptors, have been used to pattern cells and to address fundamental questions on adhesion, growth and differentiation or cell manipulation ¹¹. Fabricated via block copolymer micelle nanolithography ¹³, these culture platforms comprise patterns of gold nanodots surrounded by a cell-phobic region of PEG molecules, and are in turn functionalized with RGD or other biomolecules ¹⁴⁻¹⁶. In those experiments, nanoparticles have been used as carriers for the functional moieties and as precisely located anchoring points for the cells ¹⁴⁻¹⁶.

At the same time, it is widely reported that the underlying substratum topography influences cell behaviour ¹⁷⁻²¹. Continuous anisotropic patterns at the microscale, e.g. in the form of grooves, strongly promote cell alignment and orientation along the axis compared to the flat surfaces ¹⁷⁻²⁰. Furthermore, we have previously reported on the remarkable effects of discontinuous anisotropic silicon micro-patterns on neuron cell adhesion and growth, including common cell lines as PC12 ²² and/or primary cells ^{23,24}. Besides this, nanosized discontinuous features, e.g. in the form of pits, have been shown to significantly affect stem cell differentiation favouring a specific lineage ²¹. Although the effect of a topographical pattern on one cell type cannot be extrapolated to other cell types, the studies so far show that generally the micro-scale patterns can affect cell shape, orientation and alignment, and cytoskeletal structure, while the nanostructured patterns can influence cell functions, including adhesion, proliferation, and differentiation ²⁵. Thus, there is an increasing interest in studying the effect of hierarchical topographies that combine both micro- and nano-scale features on cell growth ²⁶⁻²⁸.

In this work, we report on a novel approach to develop hierarchically-structured cell culture platforms incorporating bioconjugated AuNPs. First, the defined hierarchical substrates comprise primary pseudo-periodic arrays of silicon microcones combined with a secondary nanoscale pattern of homogeneously deposited AuNPs terminated with bio-functional moieties. It is shown that AuNPs with tailored functionalities (i.e. oligopeptides, small molecules and oligomers) can be successfully attached onto the microstructures. Secondly, as a proof of concept, hierarchical substrates incorporating AuNPs carrying the RGD peptide (cell-binding moiety) were used to study the PC12 cell growth and differentiation. Our results show an impressive growth and NGF-induced differentiation of the PC12 cells on the nano-

micro-patterned substrates, especially at early timepoints, compared to the AuNPs-free, bare, micropatterned substrates. The exploitation of the developed methodology for the binding of AuNPs as carriers of specific bio-functional moieties onto micropatterned culture substrates for cell biology studies is envisaged.

2. Materials & Methods

2.1 Fabrication of micropatterned Si substrates

Single crystal n-type Silicon (1 0 0) wafers were subjected to laser irradiation in a vacuum chamber evacuated down to a residual pressure of 10^{-2} mbar. A constant sulfur hexafluoride (SF_6) pressure of 500 Torr was maintained during the process through a precision microvalve system. The irradiating laser source was constituted by a regenerative amplified Ti:Sapphire ($\lambda=800$ nm) delivering 150 fs pulses at a repetition rate of 1 kHz and laser fluence 0.68 J/cm^2 . The sample was mounted on a high-precision X-Y translation stage normal to the incident laser beam.

2.2 Characterization of micropatterned Si substrates

After laser irradiation, micro-structured surfaces were morphologically characterized by scanning electron microscopy (SEM), as previously described²². An image-processing algorithm (ImageJ, National Institutes of Health, Bethesda, MD, USA) was implemented in order to determine the topological characteristics of the microcones, including roughness ratio, height and intercone distance from top, side-view and cross-sectional SEM images (Supporting Table 1). The roughness ratio was calculated by dividing the actual, unfolded surface area of spikes by the total irradiated area. The mean value was calculated from statistics performed at 10 individual substrates.

The wettability of the substrates at the different treatment step was performed via static contact angle measurements with the sessile drop method using an automated tensionmeter. A 2 μL distilled, deionized Millipore water droplet was gently positioned on the surface, using a microsyringe, and images were captured to measure the angle formed at the liquid–solid interface. The mean value was calculated from at least five individual measurements and expressed as mean value \pm standard deviation (S.D.).

2.3 Synthesis of AuNPs

2.3.1 Synthesis of spherical gold nanoparticles

Gold nanoparticles with a diameter of 13 ± 2 nm were synthesized following well-established literature procedures^{29,30}. Briefly, a hot aqueous solution of trisodium citrate (5 mL, 2% w/v) was added to a boiling aqueous solution of sodium tetrachloroaurate (100 mL, 1 mM) under rapid stirring. Once a colour change to deep red, indicating the formation of nanoparticles, was observed, the solution was stirred for an additional 15 min. Subsequently the particle solution was removed from the

heat and left to cool to room temperature. As prepared citrate-capped AuNPs were sterile-filtered using a 0.2 μm syringe filter and stored at 4 $^{\circ}\text{C}$ until further use. Optionally particles were functionalised with Bis(p-sulfonatophenyl)phenylphosphine dihydrate dipotassium salt (BSPP) by addition of 20 mg of the solid straight into the as-prepared gold nanoparticle solution. Particles were then left to stir at room temperature overnight. BSPP-coated AuNPs were then purified by addition of brine until a blue colour was observed, followed by centrifugation (8000 rpm, 15 min) and re-dispersion in water. Particles were stored at 4 $^{\circ}\text{C}$ until further use.

2.3.2 Synthesis of rod-shaped gold nanoparticles

Gold nanorods with an aspect ratio of ~ 2.4 were synthesized following a modified seeded-growth procedure³¹. In brief, a seed solution was prepared by mixing aqueous solutions of sodium tetrachloroaurate (5 mM, 1 mL) and CTAB (0.2 M, 1 mL). Then, an ice-cold solution of sodium borohydride (0.01 M, 0.5 mL) was added drop-wise to the mixture under rapid stirring. A colour change to light brown, indicated the formation of small (1-2 nm) seed particles. The seed solution was stirred for an additional 2 min after appearance of the brown colour and used immediately after. At the same time, a growth solution was prepared by mixing aqueous solutions of CTAB (0.2 M, 14.24 mL), sodium tetrachloroaurate (5 mM, 2 mL) and silver nitrate (5 mM, 0.21 mL) at 40 $^{\circ}\text{C}$ with stirring at 250 rpm. Subsequently, an aqueous solution of L-ascorbic acid (78.8 mM, 160 μL) was added, resulting in a colour change from yellow to colourless. After 30 s, 16 μL of the seed solution were injected into the growth solution, and the stirrer bar was removed immediately. The solution was then kept at 40 $^{\circ}\text{C}$ overnight. The as-prepared gold nanorod solution was then purified from excess CTAB by two rounds of centrifugation (8500 rpm, 20 min) and re-dispersion in borate buffer (0.01 M, pH 9).

2.4 Functionalization of AuNPs with different functionalities

2.4.1 CALNN and CALNNRGD

Au NPs were functionalized with CALNN or CALNNRGD peptides via the thiol group of the cysteine^{32,33}. All throughout a 5000x molar excess of peptides was used. Briefly, BSPP-coated AuNPs (5 nM, 5 ml) were injected with aqueous solutions of CALNN or CALNNRGD (0.5 mg/mL, 133.4 μL) and shaken at 500 rpm overnight. The reaction mixture was then purified by two rounds of centrifugation (16400 rpm, 10 min, 22 $^{\circ}\text{C}$) and re-dispersed in water. Subsequently particles were shock-frozen in liquid nitrogen and lyophilized.

2.4.2 mPEG

Au NPs were functionalized by adding SH-PEG-OCH₃ (75 μL , MW = 356.5 g/mol) to a solution of BSPP coated gold nanoparticles (5 nM, 10 mL), while shaking. The mixture was shaken for 2 h at room temperature and then kept at 4 $^{\circ}\text{C}$ overnight. Functionalized gold nanoparticles were purified by three rounds of centrifugation (16400 rpm, 15 min, 10 $^{\circ}\text{C}$) and re-dispersion in Milli-Q water.

2.4.3 PEGCOOH-Nanorods

A freshly prepared SH-PEG-COOH aqueous solution (0.5 mg/mL, 2 mL, MW = 5000 Da) was added to a solution of gold nanorods (2 mL), while stirring at 500 rpm. The mixture was sonicated for 30 s and then shaken at room temperature overnight at 500 rpm. The solution was then centrifuged (8500 rpm, 16 min, 22 °C) and re-dispersed in a freshly prepared SH-PEG-COOH solution (0.25 mg/mL). The mixture was incubated for 4 h at room temperature while shaking at 500 rpm. AuNRs@PEGCOOH were then purified by two steps of centrifugation/decantation (8500 rpm, 16 min, 22 °C) and re-dispersed in borate buffer (0.01 M, pH 9).

2.5 Immobilization of AuNPs onto the micropatterned silicon substrates

For the binding of the AuNPs onto the micropatterned silicon substrates, a novel approach, termed as ‘drop evaporation after surface functionalization’ has been implemented. Accordingly, the protocol includes the following steps: activation of the substrates, their functionalization with an organosilane and finally drop evaporation of the gold nanoparticle solution.

Specifically, the micropatterned silicon substrates (of approximately 3x3 mm² surface area) have been thermally oxidized at 1000 °C for 30 min in air. This treatment results in a conformal silicon oxide layer. Substrates were in turn activated via immersion in Piranha solution [i.e. H₂SO₄:H₂O₂ = 3:1 (v/v)] for 30 min at room temperature (RT), followed by thorough rinsing with Milli-Q water and drying with nitrogen. Then, substrates were immersed in (3-Mercaptopropyl)trimethoxysilane (MPTMS) solution in dry toluene [1.85% (v/v)] for 3 h at RT followed by rinsing in toluene and ethanol (two times), drying with nitrogen and thermal annealing at 100 °C for 30 min.

For the binding of the AuNPs onto the MPTMS-functionalized surfaces, a drop of gold NP (20 µl) solution was deposited onto the MPTMS-functionalized micropatterned silicon surfaces, and left to slowly evaporate for 16 hrs. Then the substrates were then thoroughly rinsed with milli-Q water in order to remove any AuNPs that were not chemically bound. Gold nanospheres of 13 nm diameter with the following functionalities were used: CALNN (Cys-Ala-Leu-Asn-Asn), CALNNRGD (Cys-Ala-Leu-Asn-Asn-Arg-Gly-Asp), citrate groups and methoxy-PEG group (Table 1). To improve the distribution of the nanoparticles on the surfaces, gold nanoparticle solutions were diluted in ethanol in the range of 30-50% (v/v). Gold nanorods with an aspect ratio ~2.4 and functionalized with PEG-COOH were also tested.

Furthermore, RGD chemically bound onto the micropatterned silicon substrates (termed as ‘RGD-CDI micropatterned substrates’) have been used for the cell experiments. The oligopeptide KRGD (Lysine-Arg-Gly-Asp) was covalently bound onto the micropatterned substrates using the 1,1'-Carbonyldiimidazole (CDI) protocol. Specifically, substrates were activated via immersion in Piranha solution for 30 min at RT, followed by thorough rinsing with Milli-Q water and drying. Then, substrates have been immersed in a solution of CDI (SigmaAldrich) in dry acetone (0.37 M) for

3 hrs at RT followed by immersion in acetone for 20 minutes (three times). Substrates were subsequently dried with nitrogen. A drop of KRGD solution (0.5 mg/ml in water; PeptideSynthetics, Peptide Protein Research Ltd. United Kingdom) was deposited onto the substrates and left to evaporate for 16 hrs, followed by a thorough rinse with Milli-Q water.

2.6 Characterization of AuNPs

TEM images were obtained on a Hitachi H7000 transmission electron microscope operating at a bias voltage of 75 kV.

2.7 Field Emission Scanning Electron Microscopy (FESEM)

FESEM analysis was performed on a JEOL 7000 field emission scanning electron microscope with an acceleration voltage of 15 kV. Energy-dispersive X-ray spectroscopy has been performed at specific points of the substrates. Imaging was performed without the need of any metal coating.

2.8 UV-Vis spectroscopy

The plasmon resonance of the AuNPs solution was measured using a Perkin Elmer Lambda 950 UV-vis-NIR spectrophotometer. Solutions of serially diluted AuNPs in ethanol and in water (control) were measured.

2.9 Substrates for *in vitro* experiments with cells

For the cell culture experiments the following substrates have been used: i) AuNPs functionalized with the peptide CALNNRGD have been used (termed as 'RGD-NP micropatterned silicon substrates'), ii) RGD-CDI micropatterned silicon substrates, iii) collagen-coated micropatterned silicon substrates, iv) collagen-coated standard polystyrene (PS) tissue culture coverslips (positive control; Sarstedt). The substrates were sterilized via immersion in ethanol for 1 hr. For the collagen protein coating, substrates were immersed in 0.01% (v/v) type I collagen (Sigma-Aldrich Chemie GmbH, Munich, Germany) for 2 hrs at RT and washed in phosphate buffered saline (PBS) prior to culture initiation

2.10 PC12 cell culture

The rat pheochromocytoma PC12 cell line (ATCC-LGC, Rockville, MD, USA) was maintained in complete medium comprising Dulbecco's modified Eagle's medium (DMEM; Invitrogen, Grand Island, NY, USA) supplemented with 10% horse serum (HS; Invitrogen, Carlsbad, CA, USA) and 5% fetal bovine serum (FBS; Biosera, Sussex, UK) at 37°C in a 5% CO₂ atmosphere. The cells were plated at a density of 0.75×10^5 cells/ml on the various substrates under study. The cells were allowed to adhere in complete culture medium. After 24 h, the medium was replaced either with fresh complete medium or with differentiation medium [DMEM supplemented with 50 ng/ml Nerve Growth Factor (NGF); 2.5 S, Millipore, Billerica, MA, USA]. Complete or differentiation medium was replaced every 2 days.

2.11 Immunocytochemistry

After 2 and 4 days of culture (i.e. after 1 and 3 days of differentiation), the cells were fixed with 4% PFA for 15 min and permeabilized with 0.1% Triton X-100 in PBS for 3–5 min. The non-specific binding sites were blocked with 2% BSA in PBS for 30 min. The neuron-specific β III isoform of tubulin was detected by incubating the cells with the MAB1637 monoclonal antibody (1:900 in PBS–BSA 1%; Millipore, MA, USA) for 1 hr at RT and subsequent labelling with goat–anti-mouse FITC conjugate secondary antibody (1:200 PBS–BSA 2%; Biotium, USA) for 45 min at RT. The samples were then washed with PBS and mounted on coverslips with antifade reagent containing DAPI for nuclei staining (ProLong™ Gold Antifade Mountant; Thermo Fisher Scientific).

2.12 *Live/Dead assay*

The Live-Dead Cell Staining Kit (BioVision) was implemented in order to assess cell viability. At the end of the incubation time (4 days), micropatterned surfaces with cells were covered with the staining solution and incubated for 15 min at 37 °C. Cells were observed immediately under a fluorescence microscope. Healthy cells stain only with the cell-permeable Live-Dye, fluorescing green. Dead cells can stain with both the cell-permeable Live-Dye and the cell non-permeable Propidium Iodide (PI).

2.13 *Fluorescence microscopy*

Cell imaging was performed using an epifluorescence microscope coupled to a high-resolution Carl Zeiss AxioCam colour camera; $\times 10$, $\times 20$ and $\times 40$ objectives were used.

2.14 *Quantitative evaluation with image analysis*

2.14.1 *Cell counts /numbers*

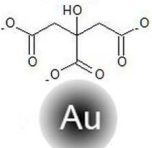
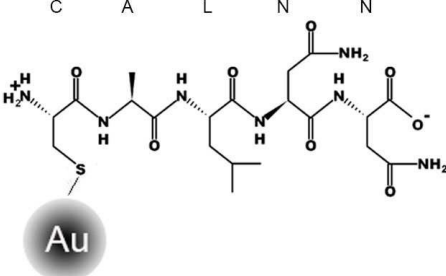
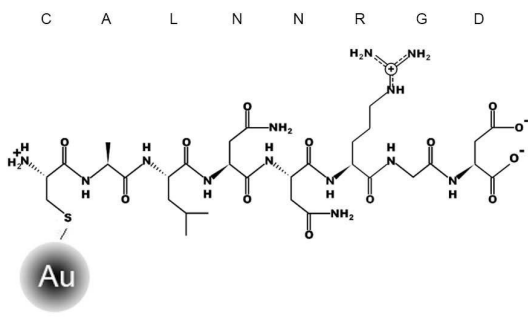
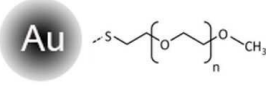
Numbers of cells grown on the various substrates were determined by counting cell nuclei stained with DAPI with ImageJ v1.36 (“Cell Counter” plugin). The results represent the means of three to five different experiments ($n = \sim 30$ fields of view for each substrate and time of culture). The data were subjected to one-way ANOVA, followed by Tukey test for multiple comparisons between pairs of means.

2.14.2 *Cell differentiation*

PC12 cell differentiation after treatment with NGF was assessed by evaluation of the differentiated cells by visual examination of the field. A differentiated cell was considered to display at least one neurite with a length equal to the cell body diameter²². Differentiation was evaluated by the length of the longest neurite and the number of neurites per differentiated cell. Neurite length, which was determined by manually tracing the contour length, was the distance from the edge of the cell soma to the neurite tip. The mean length of the longest neurite per cell was calculated. The values from all fields of views were inserted into a spreadsheet. The maximum neurite length was binned into 10 and 20 μm intervals ranging from 0 to 80 μm to generate a frequency, f , for the i^{th} interval $i=1,2,3$ (using the frequency function). Furthermore, the number of differentiated cells exhibiting 1,2,3 or >3 neurites was manually

evaluated and expressed as percent, using the frequency function. The results represent the means of three to five experiments ($n = \sim 30$ fields of view for each substrate and time of culture). The data were subjected to t-test to compare the significance differences between each condition and the control plastic substrate.

Table 1: Functionalized AuNPs

Functional group (R)	Simplified chemical structure for one R attached to AuNPs	M.W. (g/mol)
Citrate		192
CALNN (Cys-Ala-Leu-Asn-Asn)		533
CALNNRGD (Cys-Ala-Leu-Asn-Asn-Arg-Gly-Asp)		861
Methoxy-PEG Methoxy-polyethyleneglycol		365

3. Results

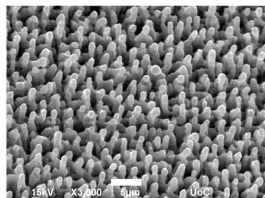
3.1 Microconical silicon substrates decorated with functionalized NPs

Micropatterning of silicon was performed by ultra-short pulsed laser structuring of crystalline silicon (Si) wafers. This technique offers the advantage of patterning Si surfaces with periodic arrays of topographical features of microscale size, while offering high accuracy and reproducibility³⁴. Upon increasing the laser energy (fluence), microconical morphologies (spikes) exhibiting different geometrical characteristics can be formed, as previously shown^{22,23}. Following surface activation via Piranha solution and functionalization via the thiol-containing silane (MPTMS), drop evaporation of the gold nanoparticles (Table 1) solution was applied.

Following this 'drop evaporation after surface functionalization' protocol (Fig. 1), the AuNPs were successfully attached to the surfaces, as confirmed by FESEM imaging. A typical example is presented in Fig. 2a, showing a top-view high magnification FESEM image of a single microcone covered with CALNN-terminated AuNPs (small bright dots). AuNPs were in the form of single particles but also in the form of small clusters. SEM-EDS elemental analysis confirmed the presence of Au onto the substrates selectively inside the region where the nanoparticle drop has been deposited (Fig. 2b and Supp. Fig. 1b).

To improve the AuNPs dispersion onto the functionalized surfaces, AuNPs solution was diluted in ethanol before the drop evaporation step. Dilution of the AuNPs solution in ethanol up to a certain ratio (v/v) significantly improved the AuNPs dispersion onto the functionalized surfaces, providing a monolayer of individual NPs in a homogenous distribution (Fig. 2c). UV-Vis spectroscopy of the respective diluted NP solutions in ethanol (v/v of 20-60%) confirmed the presence of the plasmon peak at 520 nm which coincides with the plasmon peak value of the AuNPs of 15 nm diameter (blue curve). Above a certain degree of dilution, i.e. of 70%, AuNPs were assembled onto the surface into clusters (Fig. 2e). This clustering effect occurred in the diluted solution, as indicated by the red-shift in the plasmon absorbance of the respective diluted solution (Fig. 2d – 80% dilution in ethanol and Supp. Fig. 2- 80% dilution in water, for comparison).

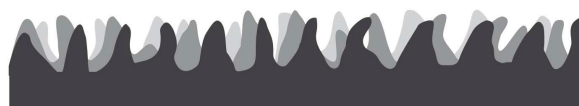
1. Ultra-short pulsed laser processing



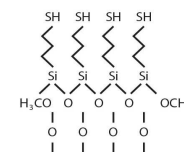
2. Surface activation & functionalization



Flat Silicon



Microconical Silicon



Functionalized Silicon

3. Drop evaporation

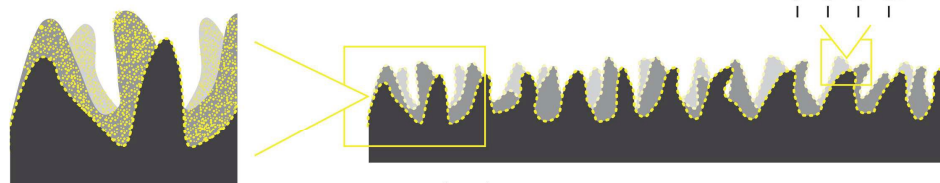
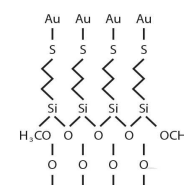
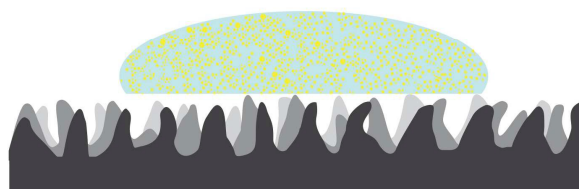
Hierarchical AuNP-
decorated microconical silicon

Figure 1: Experimental procedure of the fabrication of the hierarchical micro-nano-patterned substrates using drop evaporation after surface functionalization. SEM image of micro-patterned substrates after ultra-short pulsed laser processing (scale bar: 5 μm).

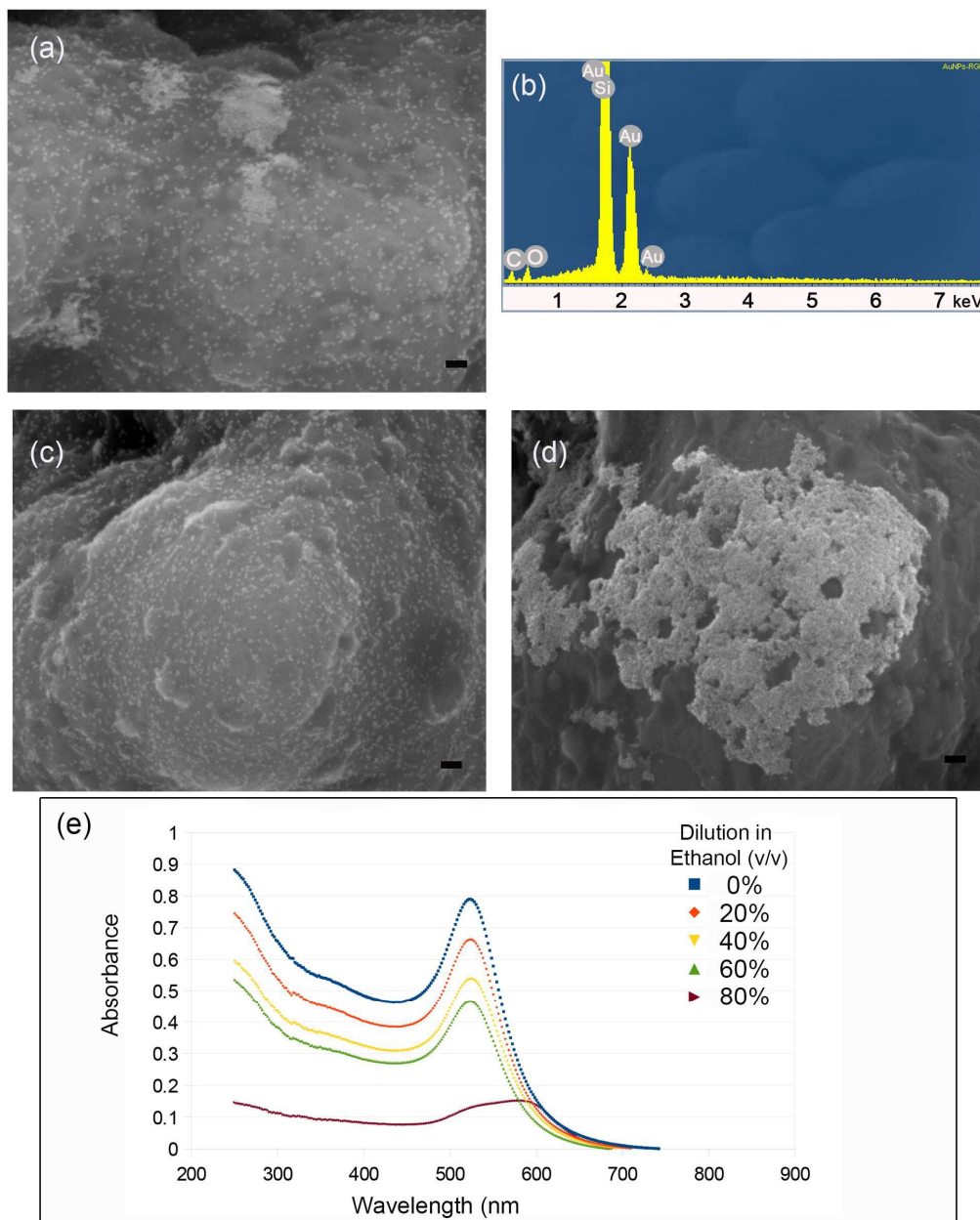


Figure 2. (a) SEM image of CALNN-terminated AuNPs, covalently bound onto micropatterned Si substrates using drop evaporation after surface functionalization (scale bar: 100 nm); (b) SEM- EDS spectra from the region shown in (a); (c-d) AuNPs deposited via the drop evaporation protocol using a solution diluted in 40 (c) and 70 (d) % of ethanol; (e) UV-Vis spectrum of the Au-NP solution diluted in increasing ratio (v/v) of ethanol.

Using the protocol of droplet evaporation after surface functionalization a plethora of AuNPs with different functionalities were successfully deposited (Figure 3). Thus,

AuNPs functionalized with oligopeptides, including CALNN (Fig. 3a,b), CALNN-RGD (Fig. 3c,d) and with small organic moieties, including the stabilizer citrate (Fig. 3e) and the methoxy-PEG group (Fig. 3f) have been chemically attached to the micropatterned substrates. Remarkably, the AuNPs could conformably disperse over the entire surface area of the microstructured substrates, covering both the 'spikes' (Fig. 3a,f) and the interspike valleys (Fig. 3c,e). Besides this, using the same protocol, AuNPs of various shapes, including spheres and rods, could be successfully attached to micropatterned substrates regardless of the type of roughness (Supporting Fig. 3).

Among the various AuNPs carrying different functionalities, Au-CALNN-RGD ('RGD-AuNPs') have been used further for the *in vitro* experiment with cells, since the oligopeptide RGD is a cell binding motif of extracellular matrix adhesion proteins. To evaluate the effect of the RGD entities carried by the gold nanoparticles, micropatterned substrates with RGD chemically attached on them have been also used in comparison. For that, KRGD oligopeptide was attached via the CDI protocol. SEM-EDS chemical elemental analysis showed carbon atom and nitrogen atom which indirectly implies the attachment of the peptide (Supporting Figure 4).

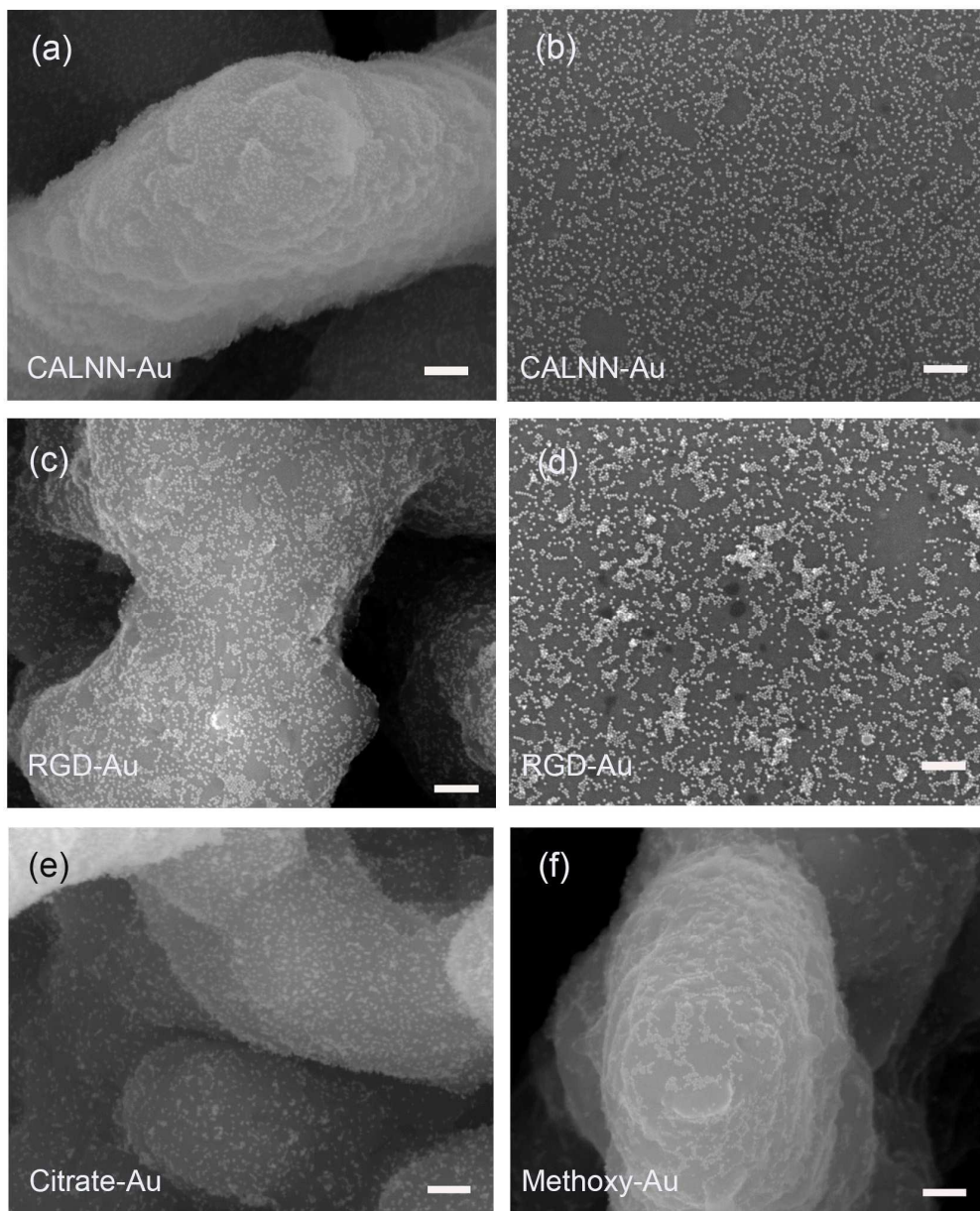


Figure 3. Top-view FESEM images of different types of Si substrates decorated with AuNPs with different functionalities via drop evaporation: (a-b) CALNN-terminated AuNPs on micropatterned (a single spike is shown) (a) and flat (b) silicon substrates; (c-d) CALNNRGD-terminated AuNPs on micropatterned (an interspike valley is shown) (c) and flat (d) silicon substrates; (e) citrate-terminated AuNPs on micropatterned (an interspike valley is shown) silicon substrates; (f) methoxy-PEG-coated AuNPs on micropatterned (a single spike is shown) silicon substrates (scale bar: 200 nm).

3.2 PC12 cell growth on the hierarchical nano-micro-patterned silicon substrates

PC12 cells were used to assess initially whether the various substrates, including the nano-micro-patterned silicon substrates with RGD-AuNP, the micro-patterned silicon substrates with RGD (RGD-CDI) and the collagen-coated micro-patterned silicon substrates (Coll-Si), could support cell growth in proliferation medium after 2 and 4 days of culture. Cell growth was assessed by immunofluorescence and SEM imaging. After 2 days, cells on the RGD-AuNPs-decorated nano-micro-patterned silicon substrates exhibited an excellent growth in the absence of any protein coating. Specifically, cells attached homogeneously in the entire substrate area as single cells, while in limited cases formed small clusters which is characteristic of the PC12 cells in the absence of NGF (Fig. 4a)³⁵. As confirmed by the Live/Dead assay, there were only a few propidium iodide-positive red-stained dead cells at 4 days *in vitro* (DIV) (Fig. 4b). PC12 cells already at 1DIV showed an excellent growth, although fewer in number (data not shown); a typical SEM view of such cells is presented in Fig. 4d. Quantitative evaluation of the cell growth via measuring the nuclei number showed that the PC12 cell growth on the RGD-AuNPs-decorated nano-micropatterned substrates was comparable to that on the positive control plastic petri dishes (Coll-plastic), which had been coated with collagen (Fig. 4c). Specifically, cell growth on the RGD-AuNPs spikes increased by 66.0% from 2 to 4DIV, while the respective increase on the collagen-coated plastic was 60.6%. On the contrary, cells cultured on the RGD moieties which had been covalently bound onto spikes using the CDI protocol (RGD-CDI) exhibited inferior growth at 2DIV, but the average cell number/surface area significantly increased within the 4DIV; though with high statistical variance. Cells on the collagen-coated micropatterned silicon substrates exhibited significantly more cells compared to the RGD-CDI at 2DIV and less at 4DIV.

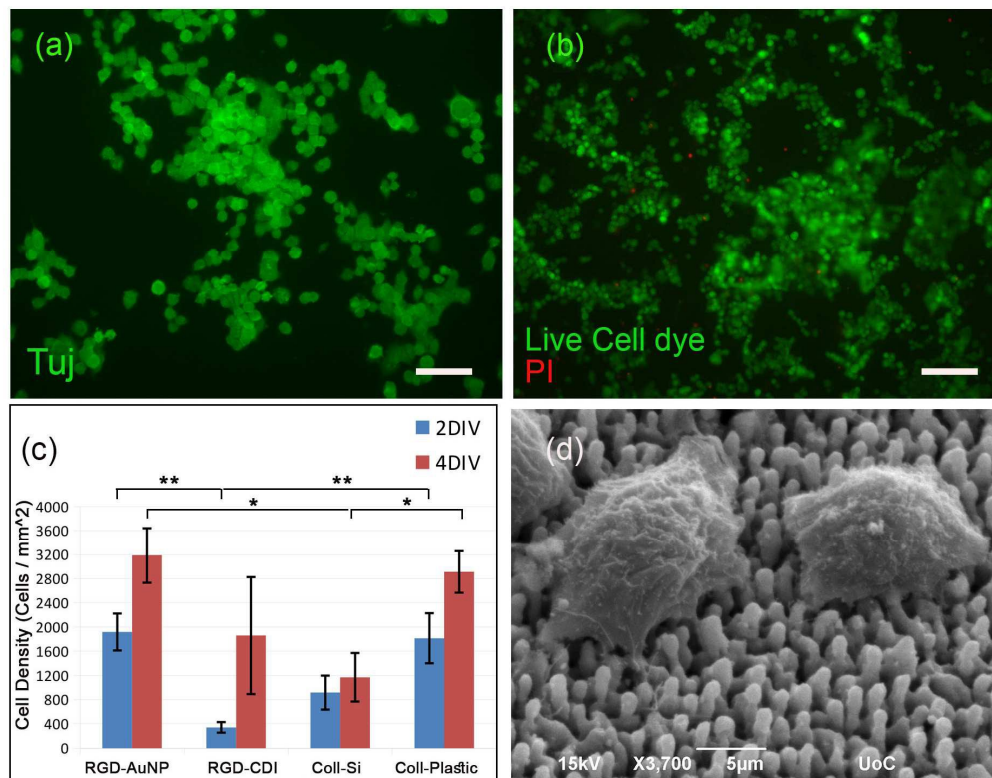


Figure 4. PC12 cell growth in proliferation medium: (a) Fluorescence microscopy images of Tuj1-positive PC12 cells grown on RGD-terminated AuNPs on micropatterned silicon substrates for 2 DIV (scale bar: 50 μm); (b) Fluorescence microscopy images of live (green) and dead (red) PC12 cells grown on RGD-terminated AuNPs on micropatterned silicon substrates for 4 DIV (scale bar: 100 μm); (c) Cell growth on the various culture substrates investigated, expressed in terms on cell number per unit area (mm²); the results represent the means of three to five different experiments (*: p < 0.05; **: p < 0.01); (d) SEM image (45° tilted view) of PC12 cells on the RGD-terminated AuNPs on micropatterned silicon substrates. (Abbreviations: RGD-AuNP, micropatterned Si substrates decorated with RGD-terminated AuNPs; RGD-CDI, micropatterned Si substrates decorated with RGD oligopeptide via CDI protocol; Coll-Si, micropatterned Si substrates coated with collagen; Coll-Plastic, plastic dishes coated with collagen).

3.3 PC12 cells differentiation on hierarchical/nano-micro-patterned silicon substrates following NGF treatment

PC12 cells were induced to differentiate towards the neuronal lineage by stimulation with NGF (50 ng/ml), which is widely used as inducer of PC12 cells differentiation into a sympathetic neuronal phenotype³⁵. PC12 cells on the RGD-AuNP-decorated micropatterned silicon substrates flattened and started to exhibit neurite extension (Fig. 5a,d). As confirmed by the Live/Dead assay, the majority of differentiated cells on the RGD-AuNP-decorated micropatterned silicon substrates at 4DIV were alive (Fig. 5b). Moreover, the differentiated cell growth on these substrates was comparable to that on the plastic petri dishes used as positive control (Fig. 5c). On the contrary, cells on the RGD-CDI substrates, where the RGD has been covalently bound by the CDI protocol, exhibited inferior growth. Furthermore, similar to the case of the NGF absence (Fig. 4c), cells on the collagen-coated micropatterned silicon substrates (Coll-Si) exhibited less pronounced growth than on the RGD-AuNP decorated ones, though better than on the RGD-CDI micropatterned substrates (Fig. 5c).

Remarkably, PC12 cell differentiation on the RGD-AuNP-decorated micropatterned substrates took place already at 2DIV (i.e. after 1 day in differentiation medium). Almost half of the differentiated cells (i.e. ~54%) extended neurites of 20-40 μm , and approximately 24% of cells exhibited neurites of greater than 40 μm length (Fig. 5e). At 4DIV (i.e. after 3 days in differentiation medium) 39% of the differentiated cells extended neurites of 20-40 μm and approximately 29% of cells exhibited neurites of greater than 60 μm length, while the respective percentage for the cells on the control plastic (Coll-Plastic) were 31% and approximately 31%, respectively. In the case of the collagen-coated micropatterned substrates (Coll-Si), the neurite length of the majority of the differentiated cells was shifted towards smaller values (Fig. 5e). Specifically, 75% of the differentiated cells at 2DIV and 59% at 4DIV exhibited neurites of 20-40 μm . Only 3.5% of the differentiated cells at 4DIV expressed neurites longer than 60 μm length. This was also the case for the RGD-CDI substrates, in which the differentiated cells extended shorter neurites. Specifically, at 4 DIV, 22% of the differentiated cells expressed neurites of 10-20 μm , 30% of the differentiated cells extended neurites of 20-40 μm , but approximately 5% of cells exhibited neurites of greater than 60 μm length (Fig. 5e).

Regarding the neurite branching, the majority of the differentiated cells exhibited 2 neurites per cell regardless the micropatterned substrate (84%, 100% and 86 % on the RGD-NP, collagen-coated and RGD-CDI substrates, respectively - Supp. Fig. 5). On the contrary, 55.1% of the cells on the collagen coated plastic flat substrates exhibited two neurites per cell and 44.9% three or more (Supp. Fig. 5).

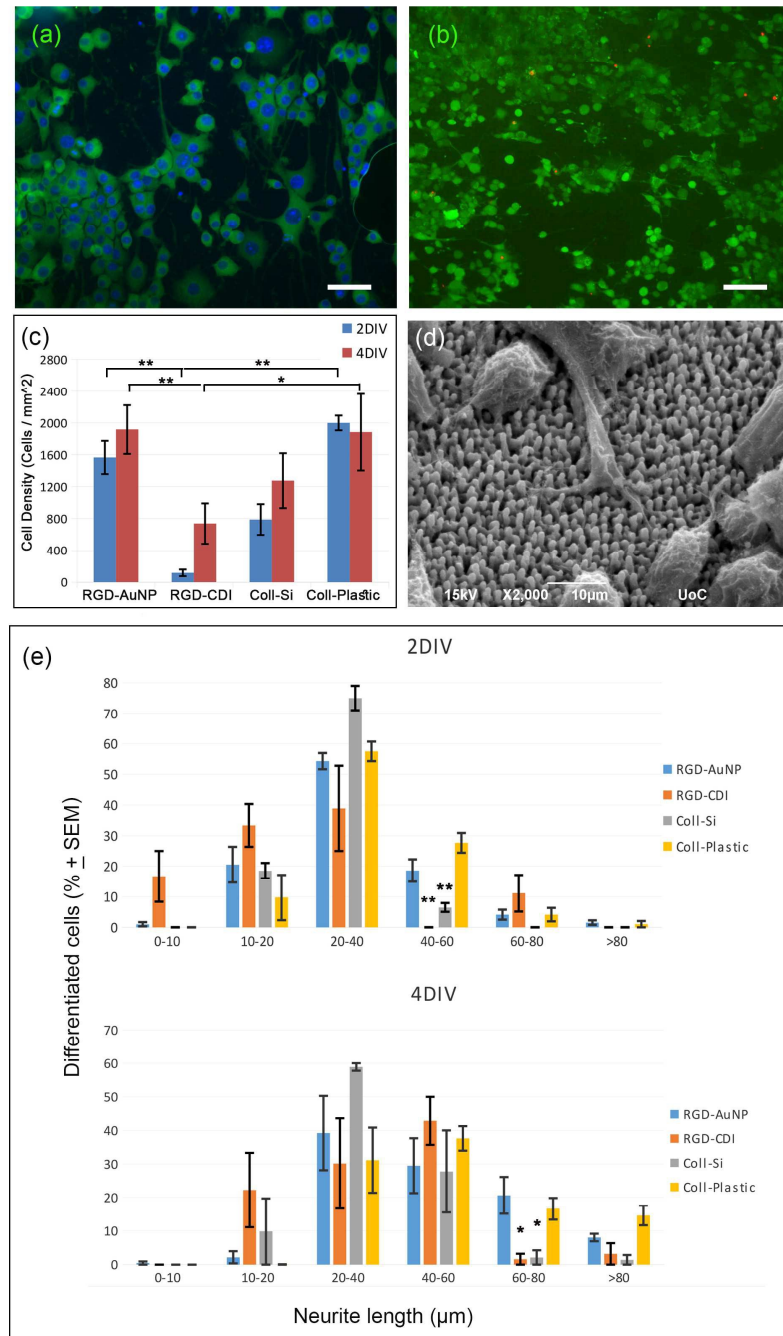


Figure 5. NGF-induced PC12 cell differentiation: (a) Fluorescence microscopy images of Tuj1-positive PC12 cells grown on RGD-AuNPs nano-micropatterned silicon substrates for 4 DIV (scale bar: 50 μm) and DAPI-stained nuclei (blue); (b) Fluorescence microscopy images of live (green) and dead (red) PC12 cells grown on RGD-AuNPs-decorated nano-micropatterned silicon substrates after 4DIV (scale bar: 100 μm); (c) Cell growth on the

various substrates tested, expressed in terms of cell number per unit area (mm^2) on 2 and 4 DIV. The results represent statistics from three to five different experiments. (*: $p < 0.05$, **: $p < 0.01$); (d) SEM image (45° tilted view) of NGF-treated PC12 cells on micropatterned silicon substrates decorated with RGD-terminated AuNPs at 2DIV; (e) Neurite length of the differentiated PC12 cells on the various substrates tested for 2 and 4DIV. The number of cells exhibiting a neurite length value within a specific range is expressed as percentage of cells \pm standard error of the mean (SEM); the results represent statistics from three to five different experiments (*: $p < 0.05$, **: $p < 0.01$).

4. Discussion

The fabrication of plasmonic substrates comprising AuNPs attached or grown in a precise manner onto substrates has recently attracted increasing scientific interest. Plasmonic substrates can be exploited towards introducing new conceptual approaches and applications in biosensing^{19,36,37} and cell biology studies^{14–16}. Immobilization of individual NPs on various surfaces, exhibiting a homogenous distribution, is a critical step that dictates the performance of such systems. Indeed, NP aggregate formation affects the underlying properties of the substrate in a negative way, e.g. in the case of bioanalytical SERS applications. The most commonly used methods to attach NPs on surfaces are the chemically-assisted^{37–40} and drying-mediated assembly⁴¹. Despite the numerous studies, drying-mediated deposition of NPs seems to be rather complex^{42–45}. While the chemically assisted method has been studied only on a small scale to structured substrates³⁸. However, it requires relatively high solution volumes. In this study, a novel method combining the chemical-assisted and the drying-evaporation assembly protocols, has been developed to successfully bind individual functionalized NPs, in a homogenous dispersion, onto micropatterned substrates. The method includes the surface activation and functionalization of the surfaces using the MPTMS silane followed by drop evaporation of nanoparticles solution. This novel protocol exploits the advantages of both assembly protocols, i.e. chemical binding of the nanoparticles via a silane coupling agent, and limited amount of nanoparticle suspension volume. Furthermore, it is reproducible and applicable in nanoparticles with various functionalities (Figure 3).

Due to the chemical attachment of the nanoparticles to the MPTMS, the gold nanoparticles via the suggested protocol are proven to be more stable compared to the drop evaporation protocol. SEM imaging of the substrates before and after thorough rinse with water showed homogenous distribution of single nanoparticles. On the contrary, SEM imaging of substrates which had not been activated with the MPTMS, showed that any attached nanoparticles were rinsed off after rinse (data not shown). Furthermore, AuNPs attached via the presented protocol were stable onto the micropatterned substrates even after four days in cell culture (Supp. Figure 6). Although the substrates were immersed in growth medium (and cells were grown onto

them), and sequentially fixated, dehydrated and critical point dried, the gold nanoparticles were still visible on the micropatterned silicon surfaces.

Our platform exhibits a hierarchical topography at the micro- and nano-scales provided by the microcones together with the homogeneously dispersed AuNPs, respectively. At the same time, it exerts a cell-binding functionality, stemming from the RGD oligopeptide end group of the AuNPs. In our previous work, we studied the effect of microscale topography on the proliferation and differentiation of PC12 cells²². The substrates developed in the present work enabled the investigation of the effect of the combined effects of hierarchical topography and RGD chemistry on PC12 cell growth and differentiation. Besides this, the targeted use of AuNPs as carriers of tailored bio-functional moieties provides a unique platform for further cell biology studies. Indeed, in the presence of NGF PC12 cells on the hierarchical substrates comprising RGD-functionalized AuNPs showed increased proliferation and differentiation. At the same time, cells on the RGD (using bioconjugation protocol) and collagen-coated micropatterned substrates showed an inferior differentiation behavior, in terms of neurite extensions' length. These results suggest that the RGD functionality is superior when NPs are used as carriers, compared to RGD or collagen coatings. Furthermore, among the three substrates studied, the cell growth on the RGD-Au NP coating of the micropatterned substrates exhibited the highest intra-experiment (i.e. a homogenous cell growth within the substrate) and inter-experimental reproducibility.

RGD has been recognized as a cell binding motif of many adhesion proteins of the extracellular matrix, including fibronectin, vitronectin, laminin and under some conditions, collagens⁴⁶. Various bioconjugation strategies have been implemented to either graft/incorporate the RGD or RGD-containing oligopeptide in the biomaterial bulk^{47,48} or to immobilize it on the biomaterials surface at a post-processing stage^{47,49–52} for diverse biomaterials and tissue engineering applications. Binding the small functional oligopeptide instead of the whole macromolecular chain becomes especially important in the case of micro and/or nano-rough surfaces or implant surfaces, where non-uniform surface adsorption of proteins can take place⁵³. In this study, we compare our novel way to immobilize RGD onto micropatterned substrate with a well-established bioconjugation protocol (via CDI) which is commonly used to immobilize amine-containing molecules. The difference in terms of the cell growth implies the superiority of our introduced protocol for the specific micropatterned substrates. The interpretation of the results can be attributed to the different chemical reactions involved in the two protocols. In the bioconjugation protocol, the surface is functionalized with CDI, by giving an active intermediate (imidazole carbamate)⁵⁴. Then the peptide binds to the intermediate by the dissociation of the hydrogen atom of its N-H group. In our protocol, the surfaces are functionalized with MPTMS. The hydrogen atom is then dissociated from the S-H (sulfhydryl group/thiol group) and the sulphur atom binds with a gold atom of the gold nanoparticles. Taking into consideration, that the S-H dissociation energy of the thiol is lower than that of the N-H group of a primary amine (353 and 377 kJ/mol at 25 °C, respectively), the

corresponding reaction of our protocol is more favourable than the other, leading to superior RGD functionality. Furthermore, the gold nanoparticles are more effective carriers of the RGD units in terms of quantity. One gold nanoparticle comprises many gold atoms some of which are functionalized by RGD oligopeptides. When deposited onto the silicon which has been functionalized with the MPTMS, one gold atom of the gold nanoparticle reacts with one sulphur atom of one MPTMS molecule. Thus, we could say that there is a kind of amplification in terms of the quantity of the RGD units carried by the gold nanoparticles.

It is also understood that apart from the surface chemistry, the surface topography can influence the kinetics of protein adsorption and the structure and conformation of the adsorbed proteins^{53,55,56}. Therefore, a well-controlled deposition of functional moieties will assist towards dictating cell adhesion and subsequent cell responses. Our findings reveal that neurite branching is practically influenced by the surface micro-scale topography, rather than by the surface chemistry. Indeed, regardless of the type of the micropatterned substrate used, differentiated cells exhibited a similar number of neurite extensions, i.e. two. On the contrary, cells on the flat control substrates exhibited either two or three neurite extensions.

The present study suggests AuNPs as precise and reliable carriers of biofunctional moieties, which can be selectively immobilized in a controlled manner onto micropatterned surfaces. As a proof of the improved functionality, it is shown that RGD units carried by AuNPs lead to superior PC12 cell growth and differentiation compared to RGD deposited in the form of bioconjugation protocol. Work using AuNPs of different functionalities is under progress, to clarify whether this effect comes from the nanoroughness imposed by the AuNPs, the RGD functionality itself or the synergy of both.

CONCLUSION

In this work, a simple protocol – drop evaporation after surface functionalization - to realize uniform monolayers of single AuNPs onto both the flat and the micropatterned silicon surfaces is developed. Using this protocol, we showed that AuNPs could be evenly dispersed throughout the entire micropatterned surface area. The protocol has been validated with different AuNPs shapes, as well as with AuNPs carrying different functional moieties. It is demonstrated that AuNPs can be used as precise and reliable carriers of biofunctional moieties, which can subsequently be selectively immobilized in a controlled manner onto micropatterned surfaces. As a result, the biological effect of RGD molecular units, carried by AuNPs immobilized on micropatterned surfaces, on PC12 cell proliferation and differentiation has been significantly improved. The exploitation of this protocol to create functional cell culture platforms for further applications in cell biology is highly envisaged.

Acknowledgements

This work was supported by the European Research Infrastructures NFFA-Europe and Laserlab-Europe, funded by EU's H2020 framework programme for research and

innovation under grant agreements n. 654360 and 654148 respectively. The authors also gratefully acknowledge the use of facilities of Prof. Vamvakaki lab. The help of Zografia Karekou in the design of Fig. 1 is acknowledged.

5. References

1. L. A. Dykman & N. G. Khlebtsov. *Acta naturae*, 2011, **3**, 34–55
2. E. Boisselier & D. Astruc. *Chemical Society Reviews*, 2009, **38**, 1759–1782
3. P. Podsiadlo, V. A. Sinani, J. H. Bahng, N. W. S. Kam, J. Lee & N. A. Kotov. *Langmuir*, 2008, **24**, 568–574
4. L. Hosta, M. Pla-Roca, J. Arbiol, C. López-Iglesias, J. Samitier, L. J. Cruz, M. J. Kogan & F. Albericio. *Bioconjugate Chemistry*, 2009, **20**, 138–146
5. Y.-H. Chen, C.-Y. Tsai, P.-Y. Huang, M.-Y. Chang, P.-C. Cheng, C.-H. Chou, C. DH, W. CR, S. AL & W. CL. *Molecular Pharmaceutics*, 2007, **4**, 713–722
6. S. Dhar, W. L. Daniel, D. A. Giljohann, C. A. Mirkin, S. J & S. J. Lippard. *JACS*, 2009, **131**, 14652–14653
7. D. N. Heo, W. K. Ko, H. R. Lee, S. J. Lee, D. Lee, S. H. Um, J. H. Lee, Y. H. Woo, L. G. Zhang, D. W. Lee & I. K. Kwon. *Journal of Colloid and Interface Science*, 2016, **469**, 129–137
8. A. Verma & F. Stellacci. *Small*, 2010, **6**, 12–21
9. J. A. Yang, H. T. Phan, S. Vaidya & C. J. Murphy. *Nano Letters*, 2013, **13**, 2295–2302
10. D. Bartczak, O. L. Muskens, S. Nitti, T. Sanchez-Elsner, T. M. Millar & A. G. Kanaras. *Small*, 2012, **8**, 122–130
11. J. J. Giner-Casares & L. M. Liz-Marzán. *Nano Today*, 2014, **9**, 365–377
12. B. Yan & B. M. Reinhard. *Journal of Physical Chemistry Letters*, 2010, **1**, 1595–1598
13. J. Blümmel, N. Perschmann, D. Aydin, J. Drinjakovic, T. Surrey, M. Lopez-Garcia, H. Kessler & J. P. Spatz. *Biomaterials*, 2007, **28**, 4739–4747
14. S. Li, X. Wang, B. Cao, K. Ye, Z. Li & J. Ding. *Nano Letters*, 2015, **15**, 7755–7765
15. M. Arnold, E. A. Cavalcanti-Adam, R. Glass, J. Blümmel, W. Eck, M. Kantslehner, H. Kessler & J. P. Spatz. *ChemPhysChem*, 2004, **5**, 383–388
16. J. Deeg, M. Axmann, J. Matic, A. Liapis, D. Depoil, J. Afrose, S. Curado, M. L. Dustin & J. P. Spatz. *Nano Letters*, 2013, **13**, 5619–5626
17. J. L. Charest, L. E. Bryant, A. J. Garcia & W. P. King. *Biomaterials*, 2004, **25**, 4767–4775
18. M. Lietz, L. Dreesmann, M. Hoss, S. Oberhoffner & B. Schlosshauer. *Biomaterials*, 2006, **27**, 1425–1436
19. W. Li, Q. Y. Tang, A. D. Jadhav, A. Narang, W. X. Qian, P. Shi & S. W. Pang. *Scientific Reports*, 2015, **5**, 8644
20. M. J. Mahoney, R. R. Chen, J. Tan & W. Mark Saltzman. *Biomaterials*, 2005, **26**, 771–778
21. M. J. Dalby, N. Gadegaard, R. Tare, A. Andar, M. O. Riehle, P. Herzyk, C. D. W. Wilkinson & R. O. C. Oreffo. *Nature materials*, 2007, **6**, 997–1003
22. C. Simitzi, E. Stratakis, C. Fotakis, I. Athanassakis & A. Ranella. *Journal of Tissue Engineering and Regenerative Medicine*, 2015, **9**, 424–434
23. C. Simitzi, P. Efstathopoulos, A. Kourgiantaki, A. Ranella, I. Charalampopoulos, C. Fotakis, I. Athanassakis, E. Stratakis & A. Gravanis.

- Biomaterials*, 2015, **67**, 115–128
24. E. L. Papadopoulou, A. Samara, M. Barberoglou, A. Manousaki, S. N. Pagakis, E. Anastasiadou, C. Fotakis & E. Stratakis. *Tissue Engineering Part C- Methods*, 2010, **16**, 497–502
 25. H. J. Jeon, C. G. Simon & G. H. Kim. *Journal of Biomedical Materials Research - Part B Applied Biomaterials*, 2014, **102**, 1580–1594
 26. W. G. Bae, H. E. Jeong & J. Kim. *Materials Letters*, 2015, **159**, 213–217
 27. M. Jaggy, P. Zhang, A. M. Greiner, T. J. Autenrieth, V. Nedashkivska, A. N. Efremov, C. Blattner, M. Bastmeyer & P. A. Levkin. *Nano Letters*, 2015, **15**, 7146–7154
 28. K. Kubo, N. Tsukimura, F. Iwasa, T. Ueno, L. Saruwatari, H. Aita, W. A. Chiou & T. Ogawa. *Biomaterials*, 2009, **30**, 5319–5329
 29. J. Turkevich, P. Cooper Stevenson & J. Hillier. *Discussion of the Faradaic Society*, 1951, **11**, 55–75
 30. G. Frens. *nature physical science*, 1973, **241**, 20–22.
 31. B. Nikoobakht & M. A. El-Sayed. *Chem. Mater.*, 2003, 1957–1962
 32. R. Lévy, N. T. K. Thanh, R. C. Doty, I. Hussain, R. J. Nichols, D. J. Schiffrin, A. Mathias Brust & D. G. Fernig. *JACS*, 2004, **126**, 10076–10084
 33. R. Fernandes, N. R. Smyth, O. L. Muskens, S. Nitti, A. Heuer-Jungemann, M. R. Arden-Jones & A. G. Kanaras. *Small*, 2014, **11**, 713–721
 34. E. Stratakis. *Sci Adv Mater*, 2012, **4**, 407–431
 35. L. A. Greene & A. S. Tischler. *PNAS*, 1976, **73**, 2424–2428
 36. C. Farcau, M. Potara, C. Leordean, S. Boca & S. Astilean. *Analyst*, 2013, **138**, 546–552
 37. N. I. Evcimen, S. Coskun, D. Kozanoglu, G. Ertas, H. E. Unalan & E. N. Esenturk. *RSC Advances*, 2015, **5**, 101656–101663
 38. D. Lin, Z. Wu, S. Li, W. Zhao, C. Ma, J. Wang, Z. Jiang, Z. Zhong, Y. Zheng & X. Yang. *ACS Nano*, 2017, **11**, 1478–1487
 39. K. Fujiwara, H. Kasaya & N. Ogawa. *Analytical Sciences*, 2009, **25**, 241–248
 40. S. Gilles, C. Kaulen, M. Pabst, U. Simon, A. Offenhäusser & D. Mayer. *Nanotechnology*, 2011, **22**, 295–301
 41. W. Han, B. Li & Z. Lin. *ACS Nano*, 2013, **7**, 6079–6085
 42. K. Kondiparty, A. Nikolov, S. Wu & D. Wasan. *Langmuir*, 2011, **27**, 3324–3335
 43. G. Puliti, S. Paolucci & M. Sen. *Applied Mechanics Reviews*, 2012, **64**, 1–23
 44. M. Parsa, S. Harmand, K. Sefiane, M. Bigerelle & R. Deltombe. *Langmuir*, 2015, **31**, 3354–3367
 45. Y. Li, F. Wang, H. Liu & H. Wu. *Microfluid Nanofluid*, 2015, **18**, 111–120
 46. E. Ruoslahti. *Annu Rev Cell Dev Biol.*, 1996, **12**, 697–715
 47. U. Hersel, C. Dahmen & H. Kessler. *Biomaterials*, 2003, **24**, 4385–4415
 48. K. Klinkhammer, J. Bockelmann, C. Simitzis, G. A. Brook, D. Grafahrend, J. Groll, M. Moller, J. Mey & D. Klee. *J Mater Sci Mater Med*, 2010, **21**, 2637–2651
 49. A. A. Sawyer, K. M. Hennessy & S. L. Bellis. 2007, **28**, 383–392
 50. M. Shachar, O. Tsur-Gang, T. Dvir, J. Leor & S. Cohen. *Acta Biomaterialia*, 2011, **7**, 152–162
 51. E. J. Tocce, S. J. Liliensiek, A. H. Broderick, Y. Jiang, K. C. Murphy, C. J. Murphy, D. M. Lynn & P. F. Nealey. *Acta Biomaterialia*, 2013, **9**, 5040–5051
 52. L. J. Bray, S. Suzuki, D. G. Harkin & T. V Chirila. *Journal of Functional*

- Biomaterials*, 2013, **4**, 74–88
53. D. F. Williams. *Journal of Materials Science*, 1987, **22**, 3421–3445
54. G. T. Hermanson. 2008.
55. D. D. Deligianni, N. D. Katsala, P. G. Koutsoukos & Y. F. Missirlis. *Biomaterials*, 2001, **22**, 87–96
56. A. C. De Luca, M. Zink, A. Weidt, S. G. Mayr & A. E. Markaki. *J Biomed Mater Res A.*, 2015, **103**, 2689–2700